2021

Flow Characterization In Mine Ventilation Fan Blade Design Using CFD

Flow Characterization in Mine Ventilation Fan Blade Design Using CFD

Anwar Endris Hassen

FDRE Ministry of Mines and Petroleum, Research and Development Directorate, Addis Ababa, Ethiopia

Abstract

In axial ventilation fans, the generation of a uniform flow velocity is desirable for better efficiency. To that end, different fan blade types have been developed to achieve better flow uniformity. This article aimed to characterize the flow distribution and its uniformity in four blade designs, namely constant chord, tapered blade, skewed blade, and tapered skewed blade, using Computational Fluid Dynamics (CFD). The study employs an iterative study where key study decisions are made as the study progresses. The study began with the selection of a blade profile for the study. A comparative study between the NACA seven-digit and four-digit series was conducted and for its higher flow throughput, the four-digit airfoil profile was selected. Next, with 30 and 40° Angle of Attack (AoA), the constant chord blade flow pattern is characterized. At 40° AoA flow disturbance and high-velocity spots were observed establishing the problem statement. Following that, three optimization strategies (tapering, skewing, and taper skewing) were applied in the design, and the flow pattern of each design was studied. Using a dispersion study a flow uniformity comparison between the models conducted. The property trade-off between three key performance indicators: efficiency, flow rate, and flow uniformity studied. The result shows an axial fan having a higher efficiency doesn't necessarily mean it has higher throughput whereas lower flow dispersion relates to the system's higher efficiency. Therefore, it can be concluded that seeking higher efficiency and flow uniformity in the design and development of axial fans comes with system throughput trade-off.

Keywords: mine ventilation, axial flow fan, tapered blade, skewed blade, CFD

1. Introduction

The mining industry highly benefits from the use of mechanical ventilation. The ventilation system aims to serve a critical role in underground mining operations through the dilution and removal of gas and dust, heat extraction, and oxygen supply for the safety of production and staff. The system has such crucial significance; it is expected to be operational 24 hours a day. Within the operation hours, the ventilation system estimated to account for one-third of the mining operation's electrical consumption [1]. With this understanding and an outlook for sustainable mining [2], the quest for higher energy efficiency in the system continues.

It is plain fact that the efficiency of the ventilation systems and the system power consumption has an inverse relation [3]. Even if in the end, the total system integration efficiency determines the power consumption of the ventilation system, every small efficiency improvement that can be achieved at the individual component level is significant. The consideration of fans as a primary component of the system is challenged by Papar et al. [4], where they recommend system-based approach instead of component-based efficiency improvement. Such arguments shape the research focus in the field where most studies conducted in mine ventilation look at energy efficiency from the system integration level. To validate the move Demirel [5] highlighted ventilation system suffers a higher efficiency reduction due to the outlet dumper's low efficiency on her review paper. However, with the rising use of more advanced control systems such as ventilation on demand, nonlinear system control, and novel intermittent approaches, the use of damper as the only flow regulator is expected to decline. This fact

leaves fans as the lowest efficient component in the system. In addition, most of the components in the system can be found on-shelf whereas fans need to be tailored with site-specific data and its design influences the selection of other components in the ventilation system. This makes fans arguably the primary component of the system.

What makes fan design more challenging than other site-specific components of the system is that the fan itself contains several parts as shown in Fig. 1 and each part has their own design control parameters. Controlled parameters in axial fan blade design include but are not limited to, blade airfoil profile, blade span, blade breadth, angle of attack, the hub to tip ratio, tip clearance, and blade number. This parameter determines the aerodynamic characteristics of the axial fan and ultimately its efficiency. Poor study of each parameter in the design process will result in various energy loss factors indicated in [6]. Hence, axial ventilation fan blade design presents a significant challenge and good research area for energy conservation. To that end, the effect of design-controlled parameters on the energy efficiency of axial fans has been scrutinized in other applications such as in electronics cooling. Yet the literature from the mine ventilation perspective is limited. [7] Present an optimization strategy by manipulating the airfoil profile to achieve better efficiency using blade element theory. Also recently Panigrahi and Mishra [8] conducted a comparative study to select an efficient airfoil profile for mine ventilation application by employing CFD. In their research Petrove and Popov [9] entertained the use of variable pitch fan blades for higher efficiency. The effect AoA has on the power consumption of the ventilation discussed by Kazakov et al. [10].

Flow distribution study in axial fans is highly important as it provides a comprehensive represen tation of the effect each control parameters have on the system. Different configurations of the controlled parameters in the design process due

Fig. 1. The schematic of axial flow fan [11].

Abbreviation	
u	circumferential velocity
r	radius
D	diameter
ω	angular velocity
q	velocity pressure
ρ	density
v	velocity
s	standard deviation
$\underline{s}$	modified standard deviation

result in different flow patterns. The manipulation of these parameters will allow the designer to seek more uniformity in the flow that is challenged by the fan wheel velocity governing equation. Equation (1) relates the fan circumferential speed (u) with the radius of the blade (r) and its angular velocity (ω). The governing equation states that a point particle at the mid radius of the fan wheel is only 25% of the velocity at the tip. Differences in speed affect the magnitude of exerted forces such as the centrifugal and shear force on different parts of the fan blade surface. Hence, the resolved forces affect the velocity triangle components resulting from deflection of discharge.

$$u = r\omega, \tag{1}$$

The velocity triangle component in turbomachinery is highly influenced by the friction coefficient of the contact surface, fluid properties, and angular velocity (ω). The circumferential speed marks its influence by creating a higher fluid shear force on the blade surface near the center of rotation due to its low circumferential speed. This leads to delayed fluid particle escape time from the working surface causing it to be highly pressurized. The pressure difference between certain portions of the blade added with centrifugal force can make the fluid particles susceptible to the pull effect the low-pressure side has at the tip.

Any fan wheel working to discharge air in the axial direction through a rotational motion cannot achieve an absolute axial discharge velocity due to the rotation speed. There must also be a rotational component creating the air deflection angle between the actual wheel velocity and axial direction. In general, when the velocity of an axial fan is studied, an axial component of the velocity triangle is referred to and it is defined as the average velocity of air moving in the axial direction through the net area of the fan in Equation (2).

Flow Velocity = Actual Flow Rate / (Throat Area − Hub Area), (2)
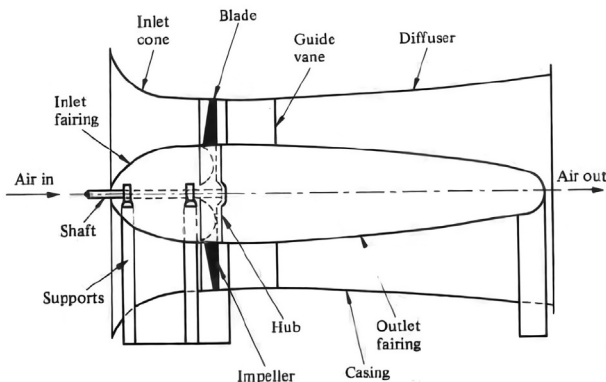
The fan wheel circumferential speed effect on system efficiency can also be observed in the velocity pressure (q) calculation of the system using Equation (3). Velocity pressure, as pertains to fans, refers to the impact of a moving air stream relative to a fixed object and is proportional to the kinetic energy. Equation (3) shows that the velocity pressure increases as a square of fan speed (υ) where the density of the working fluid (ρ) assumed constant in incompressible state. A different discharge velocity along the working surface of the fan blade when converted into velocity pressure, the lower flow velocity side will average the higher velocity side. When a system has a higher velocity pressure requires higher power to perform work, falling short when efficiency is considered. Thus it is necessary to maintain uniform discharge velocity for lower velocity pressure to avoid energy wastage and achieve higher efficiency in the system.

$$q = \frac{1}{2}\left(\rho \upsilon^2\right), \tag{3}$$

Therefore, the use of constant chord blades in axial fans will result in highly dispersed flow and lower efficiency as defined in Equations (1) and (3). To counter the problem, different types of fan blade designs emerge as a result of design control parameters manipulation. Tapered blades, curved blades (forward and backward), and skewed blades are the most common types of blades in the industry. As individual blade types with unique design parameter configuration, it is no brainer to expect a unique aerodynamic characteristic in each design model. To that end, the current study aims to inform on flow characteristics of four-blade types which are constant chord, tapered blade, skewed blade, and tapered skewed blade using CFD. The flow characterization will be conducted by employing 16 test points in the flow domain and flow velocity will be recorded at the measuring points. The recorded results will be analyzed for dispersion rate using a specially modified standard deviation formula. The effect design control parameters, in blade design, have on flow characteristics will be discussed. The study will be the first to study property trade-offs between three key performance indicators (KPI) of axial fans which are efficiency, flow rate, and flow uniformity.

2. Approach and Methods

This study aims to characterize the flow distribution in four blade designs: constant chord untwisted blade, tapered bladed, skewed blade, and tapered skewed blade. An iterative research approach was employed where key study decisions are made as the study progresses. And each blade type flow characterization was conducted and discussed by case section. The first case section mainly seeks to (a) select an airfoil profile to use in this study, and (b) establish the problem that arises when using a constant chord blade as discussed theoretically in the introduction section.

For airfoil profile selection the study relied on existing literature suggestions and a comparative study between the NACA seven and four digits series performed. Based on higher throughput generation, the airfoil profile was selected for geometry preparation in the remaining part of the study. Secondly, the first section aims to validate the statement made in the introduction section. The introduction section theoretically highlights that as the AoA increases, the bottom working surface of the blade will be exposed to large amounts of the working fluid. This will increase the drag force that will amplify the centrifugal force allowing more fluid particles to be drawn to the blade tip and escaping the surface at higher velocity. Thus, section 3.1.2a. higher blade AoA will be used to observe the phenomena graphically.

Following the selection of the airfoil profile and establishing the problem, the second case section will focus on flow characterization of the remaining blade types designed to eliminate the observed problem. Therefore, the section will use flow dispersion study as flow characterization parameters. In the flow dispersion and uniformity study, flow velocity values in the flow passage remain a vital variable. To help capture the velocity value, sixteen
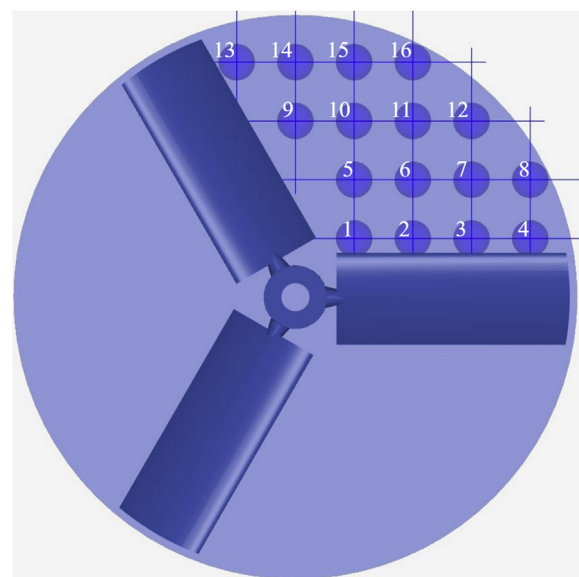

Fig. 2. Proposed test points.

probe points were applied at 0.05 m distance in the exit section of the fan blade in all models as shown in Fig. 2. The placement of the monitor points aims to get a sample representation of the blade passage flow velocity. Test point 1 is placed on the principle indicated in Equation (2) (flow velocity should be measured in the net area). The position placement of point 1 is used as a reference to set the rest of the testing points. Thus, the number of the probe points becomes the function of the net area of the flow domain, the location of the reference point, and the point separation distance. For this study the author used 0.05 m point separation, resulting in a total of 16 probe points. Since the fan wheel is expected to portray a similar flow pattern in between two consequent fan blades, the placement of the probe points in one region was found to be adequate for flow representation of the system. The probe points record the velocity of the point particle in all three dimensions independently, pressure, turbulence kinetic energy (k), and the specific rate of dissipation. Nevertheless, the probe points were able to capture different parameters, only the velocity in the axial direction will be used to perform a comparative flow dispersion study. Besides the probe points, two sample plane segments of the flow result will be used to make graphical inspection and flow rate measurement.

In general, the study contains four fan model sets with different fan geometries, where model set one contains four geometries and the remaining model set will contain two geometries each, a total of 10 geometries. Model set one will only contain a constant chord blade, the second set contains tapered blade design geometry, the third set contains the skewed blade, and the last set contains a tapered skewed blade. Fig. 3 shows a general representation of each model set blade type. A detailed design of each blade and the principle of the intended design alternation will be discussed in each case section. Care was taken to maintain general similarities with all fan designs except the parameters that remain under investigation. All fan geometries are designed with the same hub-to-tip ratio, tip clearance, and effective blade span. To maintain low hub influence on the aerodynamics performance of the system, a tapered blade neck was introduced to all geometries between the hub and the effective blade. To achieve full flow development and far-field condition, both the inlet and outlet boundaries are extended by a factor of 2D and 4D respectively, where D is the diameter of the fan wheel.

The study contains a total number of 10 geometrical models for CFD analysis and conducting a grid sensitivity study for each analysis poses to be a computationally expensive task. To obtain the acceptable mesh size, the author proposed to conduct the mesh dependency study on one randomly selected model from the geometry set. The test was conducted on tapered blade profile fan geometry with three different coarser, moderate, and finer mesh sizes containing 6.8 million, 11.8 million, and 22.1 million cells, respectively. The velocity result of the simulation at the proposed probe points compared to investigating the error margin occurs due to the difference in grid size. An average of 0.22% relative divergence deviation was recorded between the coarser and moderate mesh sizes. However, the difference margin fell to 0.09% between the last two grid sizes showing better result divergence. The same mesh development setup is used in all cases including region refinement near the rotating region to better capture the turbulence development and a local refinement of the fan blade geometry. The mesh creator algorithm's ability to automate grid sizing following the applied physics and geometry makes it difficult to obtain the same size of cell number in each case. Despite that, the remaining mesh generation operation on the rest of the model is designed to size in between the moderate and finer mesh cell count.

The same simulation setup is also used in all case sections. The problem is set on the assumption that the pressure difference created due to the rotation of the axial fan will create air movement. Therefore, the air inlet and outlet boundary condition applied with a pressure gauge value of zero pascal. The fan blade and the fan casing have a no-slip wall boundary
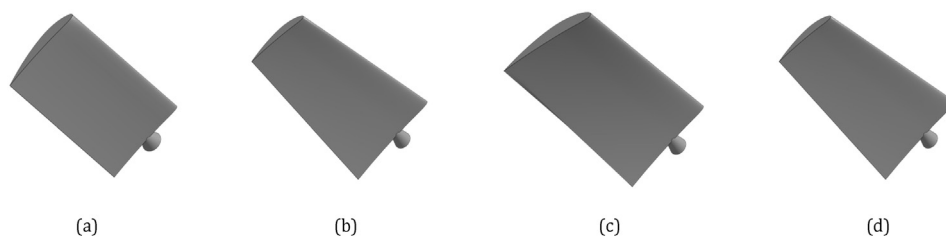

(a) (b) (c) (d)

Fig. 3. General representation of designed fan blade types: (a) constant chord, (b) tapered, (c) skewed blade, (d) tapered/twisted.

condition. With its merit of good behavior in adverse pressure gradients and capturing flow separation, the SST k-omega turbulence model with highly refined mesh should be adequate for this study. For its relatively simple yet robustness, the use of Multiple Reference Frames (MRF) was employed to model the rotating part of the problem. A study by Zadravec et al. [12] shows that the size of the rotating domain used in the MRF model influences the result. However, their study did not propose an exclusive suggestion on how to scale the domain. Thus, the author used a ratio of 1.4D and 1.1D to scale the domain height and diameter, respectively, where D is the diameter of the fan wheel. To start the problem, a fixed rotational hub speed of 50 rad/ sec was introduced to all models. The problem was solved using OpenFOAM solver, where the flow is considered incompressible and steady-state time dependent on the SimScale platform. Both the numerical results and graphical representation of the results were inspected to characterize the flow velocity distribution and to make a comparison between models. To assist the comparison, two result segments were prepared using clip filters at 0.01 m away from the fan wheel from the entry section and 0.3 m towards the exit section perpendicular to the axial flow direction. To calculate the efficiency of the fan, in the simulation a force and moment result control parameter is used. The result control parameters were able to record the useful power that is coming out of the fan which is a measure of power that the fan is producing and the measure of force imparted by the fluid on the fan blade which is equivalent to the torque required to rotate the fan wheel.

3. Results and Discussion

This chapter is structured in two major sections containing sub-sections within. The first section includes the selection of airfoil profiles that will be used for blade geometry design while flow distribution in constant chord blade type is characterized. The section also establishes a linkage between the theoretical principles highlighted in the introduction section and the CFD analysis result. Following that the second section focuses on flow characterization in blade types optimized for better flow distribution.

3.1. Constant chord blade

3.1.1. Airfoil profile selection

The selection of the CFD analysis model was the first step to begin the process. For its low computational cost requirement and simplicity, most literature employs the use of a 2D analysis model. However, even in free stream applications studies conducted by Talib et al. [13] conclude that the 2D analysis model failed to capture the full flow structure and unsteadiness of the case problem. In the current case where the ventilation fan is constructed and operates in the casing, controlled parameters such as tip clearance and boundary layer development due to the wall function of the fan duct attribute to the flow pattern. Hence, a more complex and unsteady flow structure is expected. Therefore, to best study these phenomena, a 3D analysis type is selected.

For the selection of a comparative candidate airfoil profile, the study relies on existing knowledge. To that end, after conducting a comparative study between six airfoil profiles Panigrahi and Mishra [8] concluded that a NACA 747A315 airfoil provided better efficiency. On the other hand, a summary made on the NACA airfoil series by Pier Marzocca, a professor from Clarkson University, highlights some properties that could make the seven-digit series unfavorable for ventilation applications.[1] Properties such as reduction of maximum lift coefficient and poor stall behavior as the AoA increases are mentioned as disadvantages of the series whereas the four-digit airfoil shows "good stall characteristics" that favor it for ventilation fan purposes. Therefore, NACA 747A315 and NACA 6412 were selected for comparison and the selection of the NACA 6412 airfoil profile as a candidate is arbitrary.

At the same time, the current study aims to characterize the effect AoA has on flow distribution and throughput generation. Panigrahi and Mishra's [8] study concludes the NACA 747A315 airfoil profile could perform better at 15° AoA while studies such as [14], [15] conclude a ventilation fan system could perform better at AoA range between 40 to 45°. The methods and approaches used in the studies are different and the conclusions made on both sides have good merit. Based on the suggestion an AoA of 15, 30, and 40° was selected for investigation in this study. In most comparative studies of such systems, efficiency is used as a key performance indicator. However, this study uses flow throughput as a comparison criterion because mine ventilation systems are designed based on the required flow rate. The analysis was first conducted on NACA 747A315 at 15 and 30° AoA and the 15°

---

[1] " The NACA airfoil series" https://people.clarkson.edu/~pmarzocc/AE429/The%20NACA%20airfoil%20series.pdf. Accessed 20 Apr. 2020.

AoA generated the lower throughput, hence the design dropped from further study. Following that the analysis result of 747A315 at 30° AoA compared with NACA 6412 at 30° AoA. From the comparison the NACA 6412 at 30° AoA generates a larger throughput. Therefore, the whole NACA 747A315 design set dropped and the NACA 6412 airfoil profile was selected for further investigation at AoA of 40°.

To further discuss the result obtained from each analysis, two segment planes in the inlet and exit section of the fan wheel from each analysis were studied, and the result is presented in Table 1. The use of arbitrary sampled planes to investigate results in CFD analysis has also been adopted in the different scientific literature. The bulk result at the selected section plane is calculated using the average of all cell values projected on the sampled data plane. Properties of flow rate and velocity at sectioned sample planes are used to make a numerical comparison between the two NACA airfoil families. The numerical simulation result shows a higher degree of attack was able to draw a larger throughput. The same NACA 747A315 profiled fan blade generates a 114% higher flow rate when the AoA33 increases from 15 to 30°. Moreover, the four-digit family has recorded a flow rate increment of 22% when the AoA increased to 40 from 30°. The comparison between the two families at the same AoA of 30° shows the four-digit airfoil family was able to increase the volume flow rate of the system by 10%, making it a superior choice for such application.

The fourth design in the set has presented a higher average flow velocity and a higher velocity record in the system. The increments of the maximum velocity as per the increment of the AoA in the other designs were moderate. However, the maximum velocity in design four reaches a magnitude of 28 m/s. Due to the higher average velocity, the design was able to generate a higher flow rate from the model set. However, the flow rate increment rate and system efficiency fall when compared to the first model set. This result
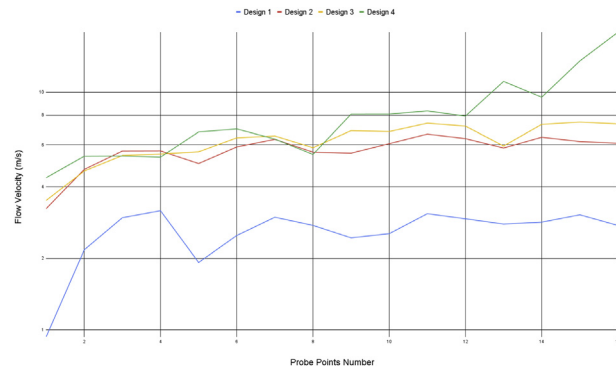

Fig. 4. Model Set 1 Axial flow velocity magnitude at probe points.

indicates the system flow distribution lacks uniformity and baleful characteristics such as noise and higher vibration may unveil in the system. The first two designs in the model set with seven-digit airfoil series have a flow rate increment of 0.03 m³/s for each 1° AoA increment from 15 to 30° and the efficiency of the system increases significantly. The last two models with the NACA four-digit record a 0.026 m³/s flow rate increment for each 1° AoA increment from 30 to 40° and its efficiency declined by almost 1%.

3.1.2. Flow distribution study in constant chord blade

Table 1 can give a clear numerical result to help make a selection decision based on the comparison of the needed volumetric flow rate. However, the numerical result alone can fall short to give the necessary information related to the main objective of this work. The introduction section highlights the effect of AoA variation on the total flow generation. To recall, it is stated that as the AoA increases, the lower surface of the blade is exposed to a higher amount of working fluid. The large exposure means a higher drag and more flow generation. The higher drag makes the rotating fluid particles more susceptible to centrifugal force where more fluid will escape to the blade tip at higher velocity. In addition, the rise of AoA more than optimum value will result in flow separation affecting performance.

Table 1. CFD analysis results calculated at the sampled data segment of Model Set 1.

Angle of Attack	Working area per blade (cm²)	Studied section (m)	NACA 747A315			NACA 6412		
			Max velocity (m/s)	Flow rate (m³/s)	Efficiency (%)	Max velocity (m/s)	Flow rate (m³/s)	Efficiency (%)
15°	369.36	0.3 inlet section	3.821	4.023e-1	51.7	—	—	—
		0.1 outlet section	3.345			—		
30°	369.36	0.3 inlet section	6.875	8.595e-1	83.59	7.901	9.435e-1	83.14
		0.1 outlet section	6.711			7.626		
40°	369.36	0.3 inlet section	—	—	—	21.6	1.209	82.41
		0.1 outlet section	—			17.45		

Therefore this section will characterize the discussed phenomena.

To help us study flow distribution, the velocity values obtained at the monitoring points are superimposed on the same graph as shown in Fig. 4. The plot shows, all designs in the model set adhered to the relation defined in the introduction section between the circumferential velocity of the fan wheel and the velocity distribution along the fan blade. The plot shows there is a lower flow velocity near the hub and increases along the blade span as the circumferential speed of the wheel increases towards the tip of the blade from probe points 1 to 4. The obtained CFD analysis result is valid as it satisfies the relation defined by the governing Equation (1). From the velocity plot, it can also be observed that a lower AoA near the hub can lead to significant flow velocity loss. As the AoA increases from 15° in design 1 to 30° in designs 2 and 3, the starting velocity values at point 1 shows a significant increment. Which indicates higher AoA near the hub could help compensate velocity loss resulted from low circumferential speed near the hub. Whereas the flow velocity at point 1 shows a slight increment when the AoA increase from 30° in design 3 to 40° in design 4, indicating the AoA reaching its optimum value and the flow starts to separate. The overall flow distribution in the first three cases shows the same flow pattern where the velocity deviation from one probe point to the next remains moderate whereas design 4 recorded undesired sudden uptake in the last four probe points indicating high-velocity spots.

In general, in both airfoil cases, a constant chord blade develops a similar flow distribution along the work surface of the blade where the flow velocity increases gradually towards the tip. However, the maximum flow velocity achieved by 40° AoA is three times higher than that of 30° AoA. The higher velocity development in the system lacks uniformity as shown in the color mapped result in Fig. 5b. The color mapped result scaled to the zone flow velocity at 2 m/s difference. The first model has four velocity zones while the second model has eight velocity zones. Since Equation (2) recommends the calculation of flow velocity only in the net area of the fan wheel, the velocity zoning at the hub and the blade can be neglected. Therefore, the model will have two velocity zones from Fig. 5a and Fig. 5b. Fig. 5a has the same flow patterns in between the working blades, yet Fig. 5b shows a different flow pattern. In the model also the flow velocity reaches up to 28 m/s in a small part of the casing corner. Such uneven flow distribution and high-velocity concentration can induce noise and vibration and result in an efficiency decrease.

3.2. Design optimization methods for optimal flow distribution

The previous section has defined the total flow distribution characteristic in a constant chord blade with different airfoil profiles and AoA. The section also highlights the larger AoA in the model set introducing undesired flow phenomena that could undercut the system efficiency. This section focuses on characterizing properties trade-off between controlled parameters and performance indicators. The flow characterization will be conducted on the most common modification strategies designed to
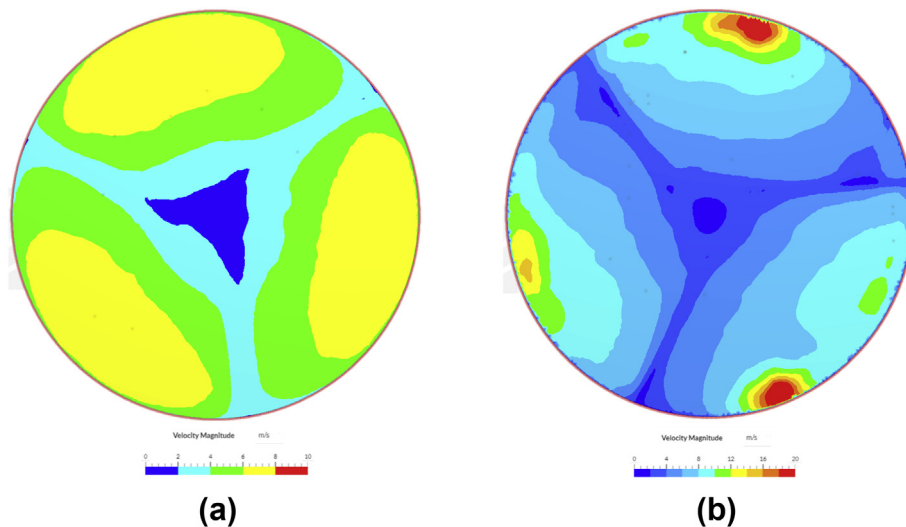

(a)   **(b)**

Fig. 5. Clip filter with velocity magnitude in the fluid flow direction: (a) AoA 30°; (b) AoA 40° (Velocity color mapping scale: 0–10 m/s for a and 0–20 m/s for b).

Table 2. Geometry description.

Model sets		Working area per blade (cm^2)	AoA in degree				chord length (mm)			
			hub	midspan	tip	difference (%)	hub	midspan	tip	difference (%)
Tapered blade	Design 1	308.82	40	40	40	0	90	75	60	33
	Design 2	328.73	40	40	40	0	90	80	70	22
Skewed blade	Design 1	366.42	40	35	30	25	90	90	90	0
	Design 2	364.23	40	30	20	50	90	90	90	0
Taper/twist blade	Design 1	308	40	35	30	25	90	75	60	33
	Design 2	328	40	35	30	25	90	80	70	22

avoid the shortcomings observed in the previous section. Efficiency, flow throughput, and flow dispersion rate will be used as KPI to characterize the system. The numerically calculated result of the defining KPI is presented in Table 3.

Equation (1) states in cases where the angular velocity remains constant, radius remains the only variable that the circumferential velocity outcome depends on. The variable radius has a uniform development from zero at the hub to full span length reaching the tip. Thus, the design of geometries containing the optimization strategies (tapering and twisting) will be dependent on the same principle where the tapper percentage and the twist angle variation from the hub to the tip will be a function of blade radius as shown in Table 2. The modification made to the geometry and the principle behind it will be discussed in detail in case sections.

The proposed probe points will be employed to perform a comparative study within the design and across the designs. The comparison across designs is straightforward, where the same positioned probe point in different designs can be compared directly and the location placement of the points will serve as a relation. However, the comparison between probe points within the same model could pose a challenge since the probe points do not have defined relations. For an optimal flow distribution, it is ideal to achieve an equal flow velocity result between the proposed probe points. In other words, the velocity value obtained at 16 test points needs to converge at the same result. However, an absolute value of zero difference between probe points cannot be achieved due to the constraints a ducted fan design comes with. The development of the boundary layer in ducted fun is the major reason. Therefore, such optimization strategies aim to achieve a minimum value of dispersion within the collected data set. For dispersion study, standard deviation statistics presented in Equation (4) are widely used.

$$s = \sqrt{\frac{\sum_{i=1}^{n}\left(x_i - \underline{x}\right)^2}{N-1}}, \tag{4}$$

$$\underline{s} = \frac{\sum_{i=1}^{n}(x_i - x_1)}{n-1}, \tag{5}$$

The measurement of dispersion in the Equation (4) is relative to the mean value ($\underline{x}$) of the data set. However, in this study optimization strategies aim to maintain similar velocity with the velocity nearest the hub. In our case, the probe point value at position 1 is the reference for the rest of the values in the data set for the dispersion study. Therefore, the mean value in Equation (4) was replaced with probe point 1 value. The square power operation of the bracket value in the standard deviation study aims to eliminate the possibility of a negative value from the subtraction operation. Since the reference value of the current data set is the smallest in the set, the operation in the bracket would not result in a negative value. Thus, the standard deviation equation was modified in the form of Equation (5) to align it with the current study objective. The operation in the dividend, the subtraction of one from the data set, will be held in the assumption of excluding the reference value (x_1) from the dispersion study because it serves as the reference value. Equation (5) creates the much-needed mathematically defined relation for velocity values obtained in the same design and serves as a comparison medium in the study.

3.2.1. Tapered blade

The surface area and velocity of the effective blade are two major factors that come into play for flow optimization in tapered blade designs. To compensate for the slower speed of the fan wheel near the hub, the tapered blade design aims to increase the chord breadth, increasing the working surface of the blade. In reverse, where the wheel velocity is higher towards the tip of the blade, the method aims to

Table 3. CFD analysis result (Efficiency, flow rate, dispersion rate).

Model sets			Average velocity (m/s)	Efficiency (%)	Flow rate (m³/s)	Dispersion rate
Constant chord/untwisted blade	Design 1	NACA 7 15°	2.544840769	51.74825175	0.402	2.2122175
	Design 2	NACA 7 30°	5.598164615	83.59447005	0.860	4.1779625
	Design 3	NACA 4 30°	6.169536154	83.14285714	0.944	4.640959167
	Design 4	NACA 4 40°	8.087791538	82.41758242	1.209	6.216591667
Tapered blade	Design 1	Tap 33	6.91232	86.18705036	1.099	4.895103333
	Design 2	Tap 22	7.139298462	83.33333333	1.138	5.191985833
Skewed blade	Design 1	Skewed 25	6.577762308	84.71698113	1.016	4.587668333
	Design 2	Skewed 50	5.420409231	87.5	0.834	3.760093333
Tapered/twisted blade	Design 1	Tap/twist 22	6.19675	86.02150538	0.973	4.491631667
	Design 2	Tap/twist 33	6.41811	85.55555556	0.999	4.621030833

decrease the surface area of the blade by decreasing the breadth of the blade profile. This design would result in surface area reduction as a variable of blade length. Thus, each blade will have a narrower blade airfoil profile at the tip where the fan while has higher speed and the airfoil profile near the hub will have a longer chord length. The optimization methods used at the National Renewable Energy Laboratory (NREL) combined experimental rotor design [16]. To investigate the optimization strategy's approach to overcoming the defined problem, design 4, from section 3.1.2., used as a benchmark.

To establish a relation with flow pattern and tapered percentage, a model set was prepared with two different geometries. The geometries are designed with NACA 6412 airfoil profile at both ends with different chord lengths. Designs 1 and 2 have chord length differences of 33 and 22%, respectively, between the larger and smaller airfoil profile as shown in Table 2. The chord length in-between remains the function of the two airfoil profiles chord lengths at both ends of the blade and the radius. The modification led to a significant reduction in the surface area of the effective blade. The selected benchmark study has a working surface area of 369.36 cm² whereas the new geometries have a surface area of 308.82 cm² and 328.73 cm² per blade in designs 1 and 2 respectively. All other geometrical features remain the same as the benchmark study with the same AoA of 40°. The same CFD simulation setup as the previous section was used to conduct the flow analysis.

For graphical inspection, the velocity color map results at 0.03 m sampled segment plane in the inlet direction presented in Fig. 5. The first design was able to generate a total of 1.096 m³/s flow rate and achieved a maximum flow of 8.988 m/s. The second model generates a 1.136 m³/s flow rate and a maximum flow velocity of 9.639 m/s recorded. The optimization method was able to cut down the sudden velocity uptake recorded at probe points 14, 15, and 16 in the benchmark model. The velocity dispersion rate within the design at recognized

probe points was calculated as 4.6 in design 1 and 5 in design 2. Hence, the applied optimization strategy was able to reduce the velocity dispersion of the system by 20.6% in design 1 and 13.7% in design 2 from 5.8 m/s velocity dispersion recorded in the benchmark design.

Looking at Fig. 6a, a significant flow velocity decrease at probe points 8 and 12 recorded and velocity uptake at point 13 observed in all models superimposed in the plot. In Fig. 4 this phenomena are observed only in design 4 and the author assumed the observed flow distribution is due to the model's high AoA characteristic. However, as presented in Fig. 6a, the same phenomena can be observed in the second model set in total alignment with the benchmark design. Through a preliminary review of the placement of the probe points and the color mapped result of the velocity distribution in Fig. 7, it can be understood that the sudden decline of velocity at probe points 8 and 12 mainly occurs due to the boundary layer development near the fan casing. Whereas the velocity uptake at probe point 13 occurs because of the placement of the probe point near the tail of the airfoil, exposing the point to a higher flow escape region. The relation governed under Equation (1) does not take into account the velocity drop and uptake that occurs due to such factors. Thus, the author proposed to exclude probe points influenced by those factors in the rest of the study. The graph is re-plotted in Fig. 6b excluding the three points and the velocity dispersion recalculated.

With the remaining 13 probe points, flow velocity difference was recalculated using Equation (5) and the benchmark design recorded a flow dispersion rate of 6.2. Designs 1 and 2 of the tapered model set recorded a dispersion rate of 4.8 and 5.1 respectively. The dispersion rate difference between the benchmark model and optimized designs calculated to be 22.5 and 17% in designs 1 and 2 respectively. Both designs improve the flow uniformity of the benchmark study. Design 1, with a higher tapering percentage, shows better flow
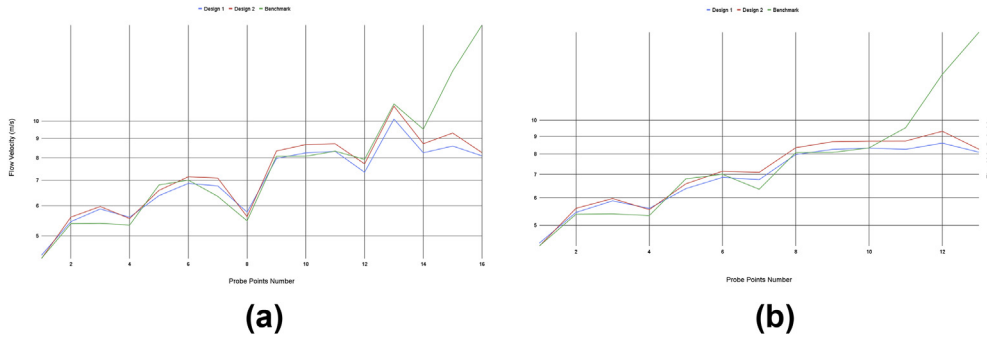
Fig. 6. Model Set 2 Axial flow velocity magnitude at the probe point: (a) 16 probe points (b) 13 probe points.

uniformity in the model set. This establishes an inverse relationship between tapering percentage and flow uniformity. As expected when the flow uniformity improved, the system efficiency also improved showing direct relation. The benchmark system has an efficiency of 82.4% design 1 and 2 recorded a system efficiency of 86 and 83%, respectively. However, system throughput generation shows an inverse relation with flow uniformity. Design 1 generates a 1.096 m³/s volumetric flow rate whereas design 2 generates a 1.138 m³/s volumetric flow rate. Therefore, it can be concluded that as the tapper percentage increases, system flow uniformity will improve and system efficiency also improved. However, system flow uniformity and efficiency improvement come at the cost of system throughput.

3.2.2. Skewed blade

The introduction of skewed angles is highly practiced in axial fan design and has been studied in detail in other sectors. Better performance in the reduction of noise [17−20] and total pressure loss [20] have been documented in published literature. Efficiency improvement is also highlighted in papers like [19, 21, 22]. In the flow velocity distribution optimization, the skewed blade principle works on defining the effective blade exposure to the air. With low AoA, the wheel blade parts the air through the blade leading edge. The aerodynamic shape of the leading edge of an airfoil is designed to have a lower surface area that results in lower exposure of the blade to the working fluid. Thus, as the fan wheel rotates at a lower angle of attack, the air deflection angle in the desired axial direction will be lower. In such cases, since the contact between the working fluid and the blade is minimal, a loss occurring due to drag will remain low. Whereas as the AoA of the working blade increases, the bottom surface of the blade that is relatively flat will be exposed to more working fluid increasing the deflection angle allowing the system to generate a higher flow rate.
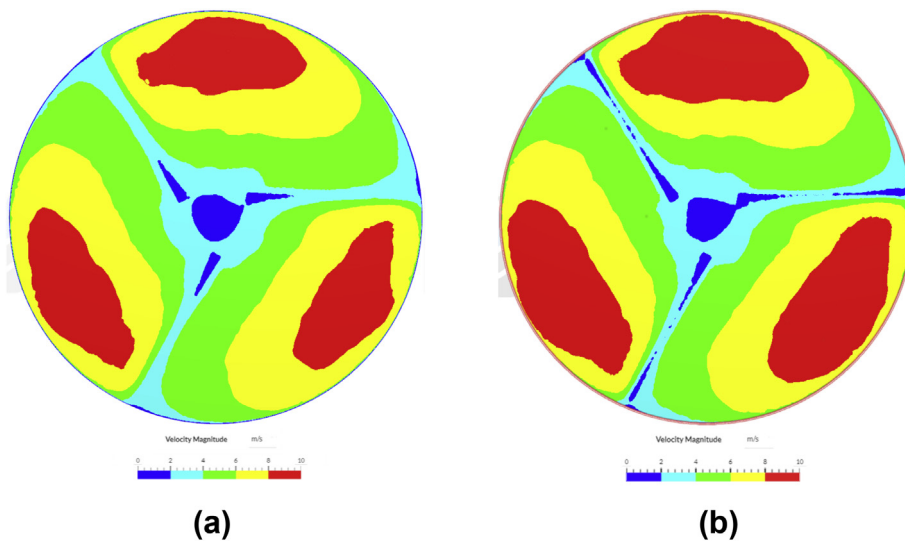

Fig. 7. Tapered blade clip filter with velocity magnitude: (a) 33% chord length difference; (b) 22% chord length difference.

The higher exposure will contribute to energy loss due to higher drag and the AoA should not be increased more than optimal to control the development of stall characteristics. Therefore, the geometry proposed for the study will have a higher AoA near the hub and decrease towards the tip of the blade and the design parameters are presented in Table 2.

Following the method used in the previous section, a model set was prepared to investigate the twist blade effect on the flow pattern. The model set contains two designs with different twist angles. The first geometry has a twist-angle blade that gradually varies from 40 to 30° AoA from the hub to the tip respectively. The second geometry has 40 to 20° AoA variation without any tapered modification. In this section, the result obtained for NACA 6412 at 40° of AoA from a model set one will be used as a benchmark. The first geometry has a surface area of $366.42\,cm^2$ per blade whereas the second geometry has a surface area of $364.23\,cm^2$ per blade. The introduction of twist angle strategy has shown a slight effective blade surface area loss when compared to the benchmark design having $369.36\,cm^2$ working area. The total number of three blades used in the design and all other geometrical features remain to be the same.

At the sampled segment, design 1 records $1.016\,m^3/s$, just over a 16% flow rate shrink from the value of the benchmark with a maximum velocity of 8.33 m/s. Design 2 generates a 31% lower flow rate from the benchmark and the maximum flow velocity recorded at probe point 11 to be 6.4 m/s. In both cases, it can be concluded that the design modification plays a significant role in the redaction of a high-pressure area near the center of rotation indicated in the benchmark study. The result exhibits the larger twist angle can cause a significant flow velocity fall affecting the average flow rate of the system. Since Fig. 8 show relatively
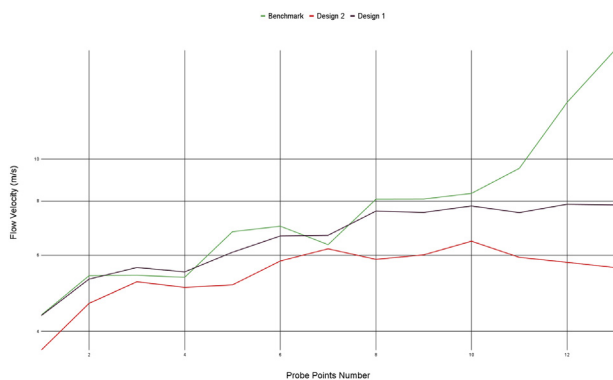

Fig. 8. Model Set 3 Axial flow velocity magnitude at probe point with benchmark.

flat trend in flow velocity, a flow uniformity improvement expected. Using Equation (5), the velocity dispersion in the system calculated and design 1 managed to reduce the total velocity difference recorded in the benchmark design by 33% while design 2 cut it by 45% achieving better flow uniformity in the model sets. Improved flow uniformity in the system has also led design 2 to achieve a higher system efficiency of 87.5%. In conclusion, as the twist angle percentage increased the system achieved lower flow dispersion and improved system efficiency. However, the optimization strategy comes with a flow rate reduction, same as tapered optimization.

3.2.3. Tapered/Twisted Blade

A tapered/twisted blade design has been used on the NREL Combined Experiment Rotors [23]. The combined design between both methods aims to trade off the characteristics that both models fall short of meeting individually. This includes the tapered blade model set achieved a higher throughput than the skewed model. And the skewed model achieved better flow uniformity than the tapered model. Now in this section, both optimization strategies will be applied on a single geometry to investigate the aerodynamic characteristics trade-off between the models.

In the skewed blade model set, design 1 has recorded higher flow velocity dispersion. By applying a tapered feature to the design, this section will investigate the change in the flow pattern. Thus, for this section, the result obtained in design 1 from a skewed model set will serve as a benchmark of the study. Following the same geometry preparation concepts as the previous section, two geometrical models were prepared for CFD analysis in this section. The first design has a twist angle that varies from 40 to 30° and a taper percentage or chord difference of 22%. The second geometry has a similar twist angle and the chord difference changed to 33%. The new geometry has not shown any significant working surface area difference for the benchmark design. Using the same CFD analysis setup, the obtained velocity in the axial direction at the measurement probe points plotted and presented in Fig. 9.

At the sampled segment of 0.03 m towards the exit direction, the design records a slight reduction in average velocity and dispersion rate from the benchmark study. Design 1 records a 6.19 m/s average velocity at the probe points showing a 5.7% reduction from the benchmark value. The dispersion rate also shows a 2.7% decrease from the 4.5 value of the benchmark. The system generate
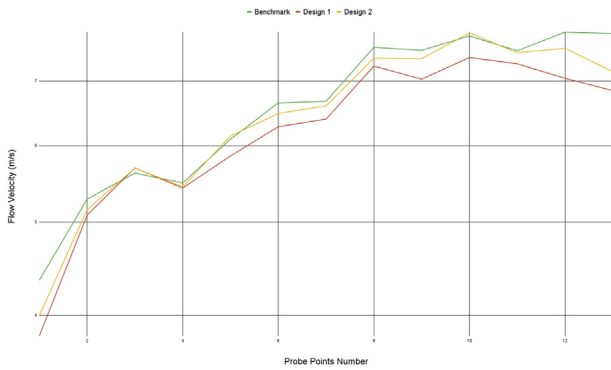
Fig. 9. Model set 4 axial flow velocity magnitudes at probe point with benchmark.

$0.973 \, \text{m}^3/\text{s}$ flow rate, showing $0.043 \, \text{m}^3/\text{s}$ flow rate decline than the benchmark study. Regarding the efficiency of the system, the design improved the benchmark study efficiency of 84.7 to 86% showing moderate improvement.

Whereas, design 2 developed an approximate value of $1 \, \text{m}^3/\text{s}$ throughput with a maximum flow velocity of 8.154 m/s recorded at the 12th probe point. The flow rate difference occurred between design 2 and the benchmark value is very small with a different percentage of 1.5%. The average flow velocity of the benchmark study within the probe point accounts 6.5 m/s while design 1 records 6.41 m/s, a 0.09 m/s difference. Even though the design shows a decrease in average velocity, the design recorded a slightly higher flow dispersion rate than the benchmark, indicating relatively disturbed flow as shown in Table 3. Design 2 recorded a velocity value that surpasses the benchmarked value at probe points 3, 5, and 10 as shown in Fig. 9 attributed to its higher flow dispersion. The system recorded efficiency of 85.5%, a 0.8% improvement from the benchmark study. However, design 2 records a lower efficiency from design 1 in the same model set. In conclusion, a tapered model set record flow uniformity and efficiency improvement as tapering percentage increase. However, in the twisted/taper model set the result was observed to be reversed where a higher tapering percentage led to flow dispersion increment and efficiency reduction.

4. Conclusion

In conclusion, through the comparison study, the four-digit NACA airfoil series was found to deliver a needed higher throughput when compared to the seven-digit family. In constant chord blade design, as the AoA increases, the flow rate of the system is also observed to increase. However, as the AoA increases more than the optimal amount, the system exhibits an undesired flow pattern affecting system efficiency. To overcome the problem, three different optimization strategies were applied and each optimization method was studied in case sections. The applied modification methods were designed with two scales in a model set. The scale difference helps to investigate improvement trends on applying optimization strategies. All optimization methods were able to eliminate the undesired flow behavior observed in the constant chord blade type. Yet the level of efficiency, flow uniformity, and throughput within each optimization method was found to be substantially different. The tapered blade type was able to cut down the sudden velocity uptake recorded at the last 4 probe points in the benchmarked study introducing normalcy in the system. However, the design comes within surface reduction, in a way it could be good for reducing fan wheel load, but also result in throughput decline. By observing the flow pattern of both designs in the tapered model set, it can be forecasted that as the tapering percentage increases, better flow distribution and higher efficiency could be achieved with the flow rate trade-off. The same conclusion can be extruded for a skewed blade model set where a higher twist angle could lead to better flow distribution and efficiency improvement, yet the method does not result in significant surface area reduction. The skewed model set was able to achieve the lowest flow velocity dispersion and higher efficiency in all designs investigated for this project. In the tapered/twisted model set, both tapered and twisted strategies were applied and the surface area reduction was the same as the tapered blade set. The strategy was found to work in reverse from a tapered model set where when the tapering percentage increased the system efficiency drops.

Conflicts of interest

None declared.

Ethical statement

The authors state that the research was conducted according to ethical standards.

Funding body

None.

author has also received editorial assistance from Carolina Giavedoni and Jousef Murad from SimScale.

Reference

[1] De la Vergne J. Hard rock miner's handbook. Edmonton: Stantec Consulting; 2008 [Online]. Available: http://www.stantec.com/content/dam/stantec/files/PDFAssets/2014/Hard%20Rock%20Miner%27s%20Handbook%20Edition%205_3.pdf. [Accessed 12 March 2021].

[2] Sterling D, Johnson G. Identifying opportunities to reduce the consumption of energy across mining and processing plants. 2010.

[3] Sharma RN. Economics of mine ventilation. Minetech 2002; 23.

[4] Papar R, Szady A, Huffer WD, Martin V, McKane A. Increasing energy efficiency of mine ventilation systems. 1999.

[5] Demirel N. Energy-Efficient Mine Ventilation Practices. Energy Effic Miner Ind 2018:287−99.

[6] Eck B. Design and operation of centrifugal, axial-flow and cross-flow fans. Oxford: Pergamon Press; 1973.

[7] Dugao Z, Jiang Z. Optimization design of an axial-flow fan used for mining local-ventilation. Comput Ind Eng 1996; 31(3−4):691−6.

[8] Panigrahi DC, Mishra DP. CFD simulations for the selection of an appropriate blade profile for improving energy efficiency in axial flow mine ventilation fans. J Sustain Min 2014; 13(1):15−21.

[9] Petrov NN, Popov NA. Ways of improving economy and reliability of mine ventilation. J Min Sci 2004;40(5):531−6.

[10] Kazakov BP, Shalimov AV, Kiryakov AS. Energy-saving mine ventilation. J Min Sci 2013;49(3):475−81.

[11] Vutukuri VS, Lama RD. Environmental Engineering in Mines. Cambridge University Press; 1986.

[12] Zadravec M, Basic S, Hribersek M. The influence of rotating domain size in a rotating frame of reference approach for simulation of rotating impeller in a mixing vessel. J Eng Sci Technol 2007;2(2):126−38.

[13] Tabib M, Rasheed A, Siddiqui MS, Kvamsdal T. A full-scale 3D Vs 2.5 D Vs 2D analysis of flow pattern and forces for an industrial-scale 5MW NREL reference wind-turbine. Energy Procedia 2017;137:477−86.

[14] Izadi MJ, Falahat A. Effect of blade angle of attack and hub to tip ratio on mass flow rate in an axial fan at a fixed rotational speed. In: Fluids Engineering Division Summer Meeting. 48401; 2008. p. 903−13.

[15] Falahat A. Numerical and experimental optimization of flow coefficient in tubeaxial fan. Int J Multidiscip Sci Eng. 2011; 2(5):24−9.

[16] Butterfield CP, Musial WP, Simms DA. Combined experiment phase 1. Final report. Golden, CO (United States): National Renewable Energy Lab; 1992.

[17] Xingshuang ZSWJW. Study on aerodynamic performance of axial flow fan with bowed blade based on Bezier function. J Huazhong Univ Sci Technol Nat Sci Ed. 2013;3.

[18] Krömer F, Müller J, Becker S. Investigation of aeroacoustic properties of low-pressure axial fans with different blade stacking. AIAA J 2018;56(4):1507−18.

[19] Ouyang H, Li Y, Du Z-H, Zhong F-Y. Experimental study on aerodynamic and aero-acoustic performance of low pressure axial flow fan with circumferential skewed blades. J Aerosp Power 2006;21(4):668−74.

[20] Cai N, Li D, Zhong F. Optimum design and experiment on skewed-swept rotating blades. J Shanghai Jiaotong Univ 1997;vol. 31:81−5.

[21] Yang L, Ouyang H, Du Z. Experimental research on aerodynamic performance and exit flow field of low pressure axial flow fan with circumferential skewed blades. J Hydrodyn Ser B 2007;19(5):579−86.

[22] Vad J, Kwedikha ARA, Horváth C, Balczó M, Lohász MM, Régert T. Aerodynamic effects of forward blade skew in axial flow rotors of controlled vortex design. Proc Inst Mech Eng Part J Power Energy 2007;221(7):1011−23.

[23] Giguere P, Selig MS. Design of a tapered and twisted blade for the NREL combined experiment rotor. Golden, CO (US): " National Renewable Energy Lab.; 1999.